

## Adsorption of ions on surfaces modified with brushes of polyampholytes

M. Borówko, S. Sokołowski, T. Staszewski, Z. Sokołowska, and J. M. Ilnytskyi

Citation: *J. Chem. Phys.* **137**, 074707 (2012); doi: 10.1063/1.4745200

View online: <http://dx.doi.org/10.1063/1.4745200>

View Table of Contents: <http://jcp.aip.org/resource/1/JCPSA6/v137/i7>

Published by the [American Institute of Physics](#).

---

### Additional information on *J. Chem. Phys.*

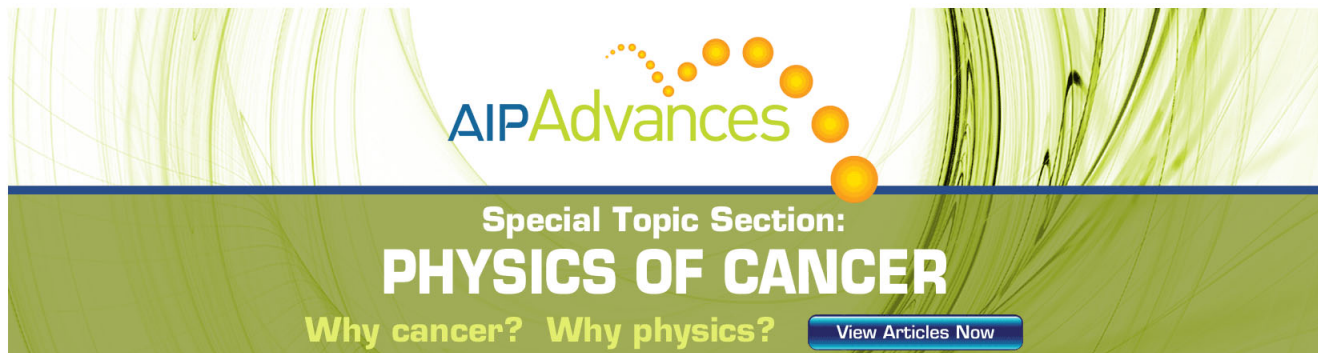
Journal Homepage: <http://jcp.aip.org/>

Journal Information: [http://jcp.aip.org/about/about\\_the\\_journal](http://jcp.aip.org/about/about_the_journal)

Top downloads: [http://jcp.aip.org/features/most\\_downloaded](http://jcp.aip.org/features/most_downloaded)

Information for Authors: <http://jcp.aip.org/authors>

## ADVERTISEMENT



**AIPAdvances**

Special Topic Section:  
**PHYSICS OF CANCER**

Why cancer? Why physics? [View Articles Now](#)

## Adsorption of ions on surfaces modified with brushes of polyampholytes

M. Borówko,<sup>1</sup> S. Sokolowski,<sup>1,a)</sup> T. Staszewski,<sup>1</sup> Z. Sokolowska,<sup>2</sup> and J. M. Ilnytskyi<sup>3</sup>

<sup>1</sup>Department for the Modeling of Physico-Chemical Processes, Maria Curie-Skłodowska University, 20-031 Lublin, Poland

<sup>2</sup>Institute of Agrophysics, Polish Academy of Sciences, Doświadczalna 4, 20-290 Lublin, Poland

<sup>3</sup>Institute for Condensed Matter Physics of National Academy of Sciences of Ukraine, 1 Svientsitskii Str, 79011 Lviv, Ukraine

(Received 13 June 2012; accepted 27 July 2012; published online 21 August 2012)

We apply density functional theory to study adsorption of ions, treated in the framework of the restricted primitive model (RPM), on surfaces modified by tethered polyampholytes. The residual electrostatic contribution to the free energy functional is approximated by using the approach proposed by Wang *et al.* [J. Phys.: Condens. Matter **23**, 175002 (2011)] for simple nonuniform RPMs systems. Our research concentrates on the problems how the distribution of the charges within chains of polyampholytes changes the selectivity of adsorption of ions species, the structure of the surface layer, and its electric properties. © 2012 American Institute of Physics. [<http://dx.doi.org/10.1063/1.4745200>]

### I. INTRODUCTION

Polyampholytes are copolymers consisting of positively and negatively charged segments. In some cases they also involve neutral segments.<sup>1</sup> A number of synthetic and natural (e.g., proteins) polymers can be classified as polyampholytes.<sup>2–6</sup> In general, two types of polyampholytes can be distinguished. In the first case charged segments carry the same amount of charge; this is a model for strongly dissociating systems. In the second case, each segment has the same, lower than 1, probability of carrying a charge; this is a model for weakly dissociating systems. Differently charged segments in polyampholytes can be distributed randomly or in a certain sequence.<sup>1,3,7–12</sup>

Bulk solutions of polyampholytes have several important applications, e.g., they can be used to stabilize colloidal mixtures and as biocompatible components for drug delivery.<sup>13,14</sup> Also, polyampholytic brushes, i.e., polyampholytes grafted by one end to solid surfaces find numerous applications, like for developing ultra-low fouling coatings, materials for selective protein adsorption and nanoactuators.<sup>15–18</sup>

Up to now, there have been a large number of theoretical studies devoted to brushes of polyelectrolytes, cf. Refs. 19–22. However, there exist much less theoretical and simulation works on polyampholyte brushes so far. Joanny<sup>23</sup> described adsorption of polyampholytes on charged and uncharged surfaces. Dobrynin *et al.*<sup>24</sup> used scaling law arguments to sketch typical adsorption regimes for polyampholytes in salt-free environments, Linse and co-authors<sup>25,26</sup> applied lattice mean field theory and Monte Carlo simulation to diblock polyampholyte brushes and studied spherical brushes of diblock polyampholytes. Baratlo and Fazli<sup>10,11</sup> investigated the effects of sequences of charged monomers on the planar semiflexible polyampholytes and effects of chain stiffness of planar diblock polyampholyte brushes. Qu *et al.*<sup>12</sup> performed

self-consistent field theory calculations to study the structure and stimuli-responsive behaviors of diblock polyampholyte brushes. Messina<sup>27</sup> applied Monte Carlo simulations to determine the behavior of polyampholytes near a charged planar surface. Computer simulations of adsorption of polyampholytes were also carried out by McNamara *et al.*<sup>28</sup>

Particularly important for theoretical studies of adsorption of chain molecules and systems involving tethered chains was the development of density functional theories (DFTs).<sup>29–33</sup> Among different approaches, the theory proposed by Wu *et al.*<sup>34–40</sup> is one of the most successful. This theory is based on the application of the first-order thermodynamic perturbation theory of Wertheim<sup>41</sup> to describe the connectivity of chains. Note that quite recently Bryk and MacDowell<sup>42</sup> developed a version of the theory that includes the second-order corrections to the thermodynamic perturbation theory.

The DFT has been also applied to study adsorption of polyelectrolytes<sup>21,22</sup> and tethered chains involving charged segments.<sup>43,44</sup> The approaches used in the above cited papers combine the theory of Wu and co-authors<sup>33,34</sup> with the density functional theories of electric double layer.

Majority of DFTs for the systems involving nonuniform ionic solutions have been based on the primitive model of electrolyte, where the solvent is considered as a structureless dielectric continuum. Although the molecular nature of the solvent is not included, the primitive model incorporates the key features of double layers: hard-sphere repulsion and the electrostatic interaction between ions.

Usual DFTs of electric double layers divide the ion-ion correlations into the direct Coulomb contribution, the hard-sphere contribution, and the electric residual contribution.<sup>45–51</sup> The difference between various approaches is mainly in the methods of evaluation of residual correlations. Typically, the residual contributions to the pair direct correlation functions are evaluated using the perturbation of the intrinsic free energy around a bulk reference state and the

<sup>a)</sup>Electronic mail: stefan.sokolowski@gmail.com.

mean spherical approximation (MSA).<sup>52,53</sup> The approaches of Refs. 45–49 can be called “compressibility route” DFTs. A more sophisticated reference fluid density theory<sup>50</sup> that applies the short-ranged MSA formulation for approximating the pair direct correlation function, but chooses a local, non-uniform fluid as the reference state instead of the bulk fluid, also belongs to “compressibility route” approaches.

In our previous papers,<sup>43,44,51</sup> we proposed the approach that uses a non-uniform fluid weighted densities as the reference state and the free energy functional for the residual contribution resulting from the MSA energy route bulk equation of state. This approach can be called as “energy route MSA-based solution”. In contrast to the compressibility route approaches, the the energy route theory was capable of predicting the gas-liquid transitions for confined ions,<sup>51,54</sup> as well as the existence of a maximum on the double layer capacity versus temperature curves.<sup>55</sup> Unfortunately, at high temperatures and for larger bulk electrolyte densities, the structure of a double layer emerging from the energy route approach is less accurate than that predicted by compressibility route theories.

Recently, Wang *et al.*<sup>56</sup> proposed a new, density functional approach for describing inhomogeneous electrolytes. Their theory also belongs to the class of “compressibility route” approaches, but uses a special weighting procedure to evaluate the change of the direct correlation function of the system relative to that of a reference state. Comparisons with Monte Carlo simulations showed that at temperatures higher than the bulk gas-liquid critical temperature, the new theory was quite accurate in predicting the ionic density profiles near a highly charged surface and was also able to capture fine features of the structural properties of the electric double layers like layering effect and the charge inversion phenomena.

In this work we combine the theory of Refs. 21 and 22 with the theory of Wang *et al.*<sup>56</sup> to study adsorption of a restricted primitive model (RPM) on surfaces covered by tethered layers of polyampholytes. In particular, we investigate how the selectivity of adsorption and the properties of the electric double layer, such as the location of the point of zero charge and the double layer capacitance, depend on the distribution of the charges along the tethered chains, on the grafting surface density and on the bulk concentration of the ionic solution. We also calculate the changes in the height of the brush with the parameters of the model.

## II. THEORY

We consider adsorption of ions on a surface modified by tethered chains. The chains ( $C$ ) are built of  $M$  tangentially jointed charged spheres of the same diameter,  $\sigma$ . The chain connectivity is assured by imposing the binding potential,  $V_b(\mathbf{R})$  (where  $\mathbf{R}$  is the set of coordinates of all the segments  $j = 1, 2, \dots, M$  within a chain), in the form given in Refs. 34–40.

Except for the first segment,  $j = 1$ , which is pinned at the surface, all remaining segments are charged. The charge of the segment  $j, j = 2, \dots, M$ , is  $Z_j^{(C)}e$ , where  $e$  is the magnitude of an elementary charge.

The fluid is modeled as a mixture of cations,  $Z_1^{(1)} > 0$  and anions,  $Z_1^{(2)} < 0$  that are charged hard spheres of the diameters  $\sigma$ . We do not explicitly consider the presence of solvent molecules, i.e., we treat the solvent as a continuum of a given (relative) dielectric permittivity  $\epsilon$ . The interactions between all the spherical species (i.e., between the segments, cations and anions) are given by

$$u_{ij}^{(\eta\alpha)}(r) = \begin{cases} \infty, & r < \sigma, \\ \frac{e^2 Z_i^{(\eta)} Z_j^{(\alpha)}}{4\pi\epsilon\epsilon_0} \frac{1}{r}, & r > \sigma \end{cases}, \quad (1)$$

where  $\eta, \alpha = C, 1, 2$ , and  $\epsilon_0$  is the permittivity of the vacuum.

The surface bonding potential of the first segment has the form

$$\exp[-v_1^{(C)}(z)/kT] = \mathcal{C}\delta(z - \sigma/2), \quad (2)$$

where  $\mathcal{C}$  is a constant. The interaction of cations, anions, and the segments,  $j = 2, \dots, M$  with the wall is described by the potential

$$v_j^{(\alpha)}(z) = v_{hw}(z) + v_{j,el}^{(\alpha)}(z), \quad (3)$$

where  $v_{hw}(z)$ , is the hard-wall potential

$$v_{hw}(z) = \begin{cases} \infty, & \text{for } z < \sigma/2, \\ 0, & \text{otherwise} \end{cases}, \quad (4)$$

and

$$\beta v_{j,el}^{(\alpha)}(z) = -2\pi l_B Q Z_j^{(\alpha)} z, \quad (5)$$

is the Coulomb potential. In the above  $\beta = 1/kT$ ,  $Qe$  is the surface charge density of the wall and  $l_B = e^2/(4\pi kT\epsilon\epsilon_0)$  is the Bjerrum length. The total chain-surface potential is the sum of the interactions of consecutive segments with the wall.

Far from the wall the fluid is uniform. The bulk densities and chemical potentials of particular species are, respectively,  $\rho_b^{(\eta)}$  and  $\mu_\eta$ ,  $\eta = 1, 2$ . The bulk densities of ionic species satisfy the electro-neutrality condition  $Z_1^{(1)}\rho_b^{(1)} + Z_1^{(2)}\rho_b^{(2)} = 0$ .

In order to proceed, we introduce the notation,  $\rho^{(C)}(\mathbf{R})$  and  $\rho_1^{(\eta)} \equiv \rho^{(\eta)}(z)$ ,  $\eta = 1, 2$ , for the density distribution of chains and of fluid species, respectively. The theory is constructed in terms of the density of particular segments of chains,  $\rho_j^{(C)}(z)$ , and the total segment density of chains,  $\rho_s^{(C)}(z)$ . These densities are introduced via commonly used relations<sup>34–40</sup>

$$\rho_s^{(C)}(\mathbf{r}) = \sum_{j=1}^M \rho_j^{(C)}(\mathbf{r}) = \sum_{j=1}^M \int d\mathbf{R} \delta(\mathbf{r}_j - \mathbf{r}) \rho^{(C)}(\mathbf{R}). \quad (6)$$

The system is studied in a grand canonical ensemble with the constraint of constancy of the number of tethered chain molecules, i.e.,

$$R_c = \int dz \rho_j^{(C)}(z), \quad (7)$$

where  $R_c$  is the total number of tethered chain molecules per area of the surface.

The equilibrium density profiles are obtained by minimizing the thermodynamic potential

$$\mathcal{Y} = F + \int d\mathbf{R} \rho^{(C)}(\mathbf{R}) \sum_{j=1}^M v^{(C)}(z_j) + \sum_{\eta=1,2} \int d\mathbf{r} [v_1^{(\eta)}(z) \rho^{(\eta)}(z) - \mu_\eta] + \int d\mathbf{r} q(z) \Psi(z). \quad (8)$$

In the above  $F$  is the free energy functional and  $q(z)$  is the charge density

$$q(z)/e = \sum_{j=1}^M Z_j^{(C)} \rho_j^{(C)}(z) + \sum_{\eta=1,2} Z_1^{(\eta)} \rho^{(\eta)}(z). \quad (9)$$

The electrostatic  $\Psi(z)$  satisfies the Poisson equation

$$\nabla^2 \Psi(z) = -\frac{4\pi}{\epsilon_0} q(z). \quad (10)$$

The solution of the differential equation (10) is given by Eq. (26) of Ref. 22. It requires denomination of the value of the electrostatic potential at the wall,  $V_0 = \Psi(z=0)$ . From the electro-neutrality condition of the system it follows that

$$Qe + \int_0^\infty dz q(z) = 0. \quad (11)$$

The principal task in density functional theory is to derive an expression for the Helmholtz energy,  $F$ , as a functional of the density profiles. Following previous works,<sup>21,22,43,44</sup> the Helmholtz energy is divided into an ideal term that depends on the bond potentials and the polymers' topology, and excesses arising from various forms of non-bonded interactions. The latter terms are responsible for the thermodynamic non-ideality. We have

$$F = F_{id} + F_{ex}, \quad F_{ex} = F_C + F_{hs} + F_{el}, \quad (12)$$

where  $F_{id}$  is the ideal contribution,

$$F_{id}/kT = \frac{1}{kT} \int d\mathbf{R} \rho^{(C)}(\mathbf{R}) V_b(\mathbf{R}) + \int d\mathbf{R} \rho^{(C)}(\mathbf{R}) [\ln(\rho^{(C)}(\mathbf{R})) - 1]. \quad (13)$$

The volume exclusion (the hard-sphere) term,  $F_{hs}$ , is calculated according to the fundamental measure theory,<sup>33</sup>

$$f_{hs}/kT = \int d\mathbf{r} \left\{ -n_0 \ln(1 - n_3) + \frac{n_1 n_2 - \mathbf{n}_{V1} \cdot \mathbf{n}_{V2}}{1 - n_3} + \frac{1}{36\pi} \left[ n_3 \ln(1 - n_3) + \frac{n_3^2}{(1 - n_3)^2} \right] \frac{n_2^3 - 3n_2 \mathbf{n}_{V2} \cdot \mathbf{n}_{V2}}{n_3^3} \right\}, \quad (14)$$

where  $n_i$ ,  $i = 0, 1, 2, 3$  and  $\mathbf{n}_{Vi}$ ,  $i = 1, 2$  are, respectively, scalar and vector total weighted densities. The total weighted densities are the sums of the weighted densities of individual species. For example,

$$n_i = n_i^{(C)} + n_i^{(1)} + n_i^{(2)}, \quad (15)$$

and  $n_i^{(C)} = \sum_{j=1}^M n_{ij}^{(C)}$ ,  $n_{ij}^{(C)}$  is the weighted density of the segments  $j$ . Because the relevant equations defining the weighted densities have been already presented in numerous works,<sup>34–40,43,44</sup> we have omitted them here.

In the case of bulk polyampholytes an expression for the free energy contribution due to chain connectivity was presented by Jiang *et al.*<sup>8</sup> On the other hand, Wang, Liang, and Wu<sup>22</sup> derived an expression for  $F_C$  applicable for describing non-uniform polyelectrolytes. The system under study differs from both systems mentioned above. The approximation for calculating  $F_C$  proposed by us results from the following arguments.

According to Wertheim's first order perturbation theory<sup>41</sup> for chains built of tangentially jointed hard spheres, the free energy  $F_C$  involves the logarithm of the contact value of the background pair correlation function,  $y_{hs}$ . A key assumption of Wertheim's approach is that  $y_{hs}$  can be represented by that corresponding to a monomeric reference system. We have

$$y_{hs} = \frac{1}{1 - n_3} + \frac{n_2 \xi \sigma}{4(1 - n_3)^2} + \frac{n_2^2 \xi \sigma}{72(1 - n_3)^3}, \quad (16)$$

where  $\xi = 1 - \mathbf{n}_{V2} \cdot \mathbf{n}_{V2}/(n_2)^2$ . In the case of adsorption of polyelectrolytes built of charged hard-spheres, each segment carries the same charge,  $Z_j^{(C)} \equiv Z^{(C)}$  for  $J = 1, \dots, M$ . This case was considered in Ref. 22. However, in our case the charges of consecutive segments can be different. Moreover, the first segment is pinned and its charge is zero, thus we have never a symmetric distribution of the charges along the chain. We propose the following approximation for  $F_C$

$$F_C/kT = -\frac{1}{2} \left[ \sum_{j=1}^{M-1} \int d\mathbf{r} n_{0j}^{(C)} \xi^{(C)} \ln y_j + \sum_{j=2}^M \int d\mathbf{r} n_{0j}^{(C)} \xi^{(C)} \ln y_j \right], \quad (17)$$

where

$$y_j = y_{hs} \times \exp \left( -\frac{1}{T^*} \frac{Z_j^{(C)} Z_{j+1}^{(C)} (2\Gamma\sigma + \Gamma^2\sigma^2)}{(1 + \Gamma\sigma)^2} \right). \quad (18)$$

In the above  $\Gamma = (\sqrt{1 + 2\kappa\sigma} - 1)/2\sigma$ ,  $T^* = \sigma/l_B$  is the "electrostatic" reduced temperature,  $\xi^{(C)} = 1 - \mathbf{n}_{V2}^{(C)} \cdot \mathbf{n}_{V2}^{(C)}/[n_2^{(C)}]^2$ , and

$$\kappa^2 = (4\pi l_B) \left[ \sum_{j=1}^M (Z_j^{(C)})^2 n_{0j}^{(C)}(z) + \sum_{\eta=1,2} (Z_1^{(\eta)})^2 n_0^{(\eta)}(z) \right]. \quad (19)$$

In the case of polyelectrolytes, Eq. (17) reduces to the equations given in Ref. 22.

Approximation (17) results from the application of "symmetrization" procedure: the segment  $j$ ,  $j = 2, \dots, M - 1$  is bonded either to the segments  $j - 1$  and to the segment  $j + 1$  and for different pairs forming bonds the contact value of the background correlation function can be different. We are aware that in our treatment the calculation of  $\Gamma$  is performed

indiscriminating the ions belonging to chains and to free ions (cf. Refs. 57–59).

Similarly to monomeric electrolyte systems, the excess Helmholtz energy arising from the coupling between the electrostatic and hard-sphere interactions is written down employing the approach described in Ref. 56. We have

$$F_{el}/kT = -\frac{1}{2} \sum_{\alpha,\eta,i,j} \int d\mathbf{r}d\mathbf{r}' \Delta \bar{c}_{ij}^{(\alpha\eta)}(\mathbf{r}, \mathbf{r}') \Delta \rho_{\alpha,i}(\mathbf{r}) \Delta \rho_{\eta,j}(\mathbf{r}'). \quad (20)$$

The summation in (20) is carried out over cations ( $\alpha$ ,  $\eta = 1$ ), anions ( $\alpha$ ,  $\eta = 2$ ), and the segments ( $i$ ,  $j = 2, \dots, M$ ) of the chains ( $\alpha$ ,  $\eta = C$ ),  $\Delta \rho_{C,i}(\mathbf{r}) = \rho_i^{(C)}(\mathbf{r})$ ,  $\Delta \rho_{1,i}(\mathbf{r}) = \rho^{(1)}(\mathbf{r}) - \rho_b^{(1)}$ , and  $\Delta \rho_{2,i}(\mathbf{r}) = \rho^{(2)}(\mathbf{r}) - \rho_b^{(2)}$ . Moreover, the functions  $\Delta \bar{c}_{ij}^{(\alpha\eta)}$  represent short-range parts of the electrostatic two-particle direct correlation functions.

Following previous publications,<sup>45–50,54</sup> we use MSA analytical expressions for the direct correlation functions and the so-called “weighted correlation approach,” WCA- $k^2$ , proposed by Wang *et al.*<sup>56</sup> We have

$$\Delta \bar{c}_{ij}^{(\alpha\eta)} = \begin{cases} 0, & r > \sigma, \\ u_{ij}^{\alpha\eta}(r) [1 - 2B_1 \frac{r}{\sigma} + B_2 (\frac{r}{\sigma})^2], & r \leq \sigma \end{cases}, \quad (21)$$

where

$$B_i(z) = \frac{\int dz' [B(z')]^i \kappa^2(z') \Theta(|z - z'| - \sigma)}{\int dz \kappa^2(z') \Theta(|z - z'| - \sigma)}, \quad (22)$$

and where

$$B(z') = \frac{1 + \kappa(z')\sigma - \sqrt{1 + 2\kappa(z')\sigma}}{\kappa(z')\sigma}. \quad (23)$$

In the above  $\Theta(|z - z'| - \sigma)$  is the step-function.

At equilibrium the density profiles minimize the thermodynamic potential  $\mathcal{Y}$ , i.e.,

$$\frac{\delta \mathcal{Y}}{\delta \rho^{(C)}(\mathbf{R})} = \frac{\delta \mathcal{Y}}{\delta \rho^{(\eta)}(\mathbf{r})} = 0, \quad \eta = 1, 2. \quad (24)$$

This condition leads to the equations

$$\rho^{(C)}(\mathbf{R}) = \mathcal{C}_1 \exp \left[ -\beta V_b(\mathbf{R}) - \beta \sum_{j=1}^M \lambda_j^{(C)}(z_j) \right] \quad (25)$$

and

$$\rho^{(\eta)}(\mathbf{r}) = \exp[\beta \mu_\eta - \beta \lambda^{(\eta)}(z)], \quad (26)$$

where

$$\lambda_j^{(C)}(z_j) = \frac{\delta F_{ex}}{\delta \rho_j^{(C)}(z_j)} + v_j^{(C)}(z_j) + e Z_j^{(C)} \Psi(z_j)$$

$$\lambda^{(\eta)}(z) = \frac{\delta F_{ex}}{\delta \rho^{(\eta)}(z)} + v_1^{(\eta)}(z) + e Z_1^{(\eta)} \Psi(z), \quad \eta = 1, 2, \quad (27)$$

and where the constant  $\mathcal{C}_1$  is calculated from the normalization condition (7). The multidimensional density profile equation (25) can be next reduced to the equations for the local densities of the consecutive segments,  $\rho_j^{(C)}(z_j)$ , by using the method described in Refs. 34–40, 43, and 44.

The theory reported above is similar to that used in Ref. 22 for nonuniform polyelectrolytes. In fact, when the averaging of Eq. (22) is not performed, our approach reduces to the latter theory. On the other hand, the calculations for simple nonuniform electrolytes demonstrated that the WCA- $k^2$  approach<sup>56</sup> is even more accurate than the usual<sup>45–49</sup> “compressibility route” theories. Also, theoretical calculations of equations of state for bulk polyampholytes carried out by Jiang *et al.*<sup>8</sup> compare well with available computer simulations data. Therefore, we can assume that the density functional results presented below should correctly capture all the discussed phenomena, at least at the qualitative level.

### III. RESULTS AND DISCUSSION

The system in question is characterized by numerous parameters. In order to reduce their number, we have already assumed that all spherical species (i.e., ions and segments) have the same size,  $\sigma$ . We also assume unit valences of all charged species,  $|Z_i| = 1$ . The value of the reduced electrostatic temperature is kept constant and equal to  $T^* = 0.5$ . This temperature is of the order of the temperature usually used in computer simulations of nonuniform electrolytes.<sup>22,56</sup> In a great majority of calculations we restrict our attention to the case when the electrostatic potential on the wall is zero,  $V_0 = 0$ .

The parameters that characterize the brush are the number of segments,  $M$ , and the surface brush density,  $R_C = R_c \sigma^2$ . The calculations are carried out assuming that the total charge of the brush is zero, i.e., that the numbers of positively and negatively charged segments are the same,  $M_+ = M_- = (M - 1)/2$ . However, the distribution of “+” and “-” charges along the chain can be different. Different distributions of charges are called the “architectures”. The first (pinned) segment is uncharged.

We introduce the following code to distinguish the systems under study. The symbol  $[m_1 + n_1 - m_2 + n_2 -, \dots]$  abbreviates a chain whose the first  $m_1$  segments (except for the pinned segment) are positively charged, the next  $n_1$ —negatively charged, and so on. When the sequence of the charges is repeated, we use parentheses to group the repeating units. For example the symbol  $[5(1 + 1 -)]$  means that the chain is built of 11 segments, the first segment is uncharged and the following segments are alternately charged with + and -.

In the case of non-modified, uncharged wall, or in the case of an uncharged wall modified with chains built of uncharged segments, no difference in adsorption of ionic species is observed, provided that ions are of the same size. The potential of zero charge (PZC) for those walls is zero. However, for differently sized ions in contact with such walls their adsorption is different. Of course, also in the case of adsorption of uncharged hard spheres of different sizes differences in adsorption of different species would occur. Therefore, the origin of different adsorption is entropic. Different adsorption of ionic species causes that PZC is different from zero.

Tethering the chains reduces the number of possible configurations of chains’ segments. For chains of different architecture the resultant charge profile will be different. Therefore, the adsorption of ionic species is expected to be

different and the selectivity of adsorption of ions, as well as PZC will depend on the architecture of chains.

Let us consider the surface modified with the chains of different architecture built of  $M = 11$  segments. The cases investigated include the systems:  $[5(1 + 1 -)]$  ( $A_{11}$ ),  $[5 + 5 -]$  ( $B_{11}$ ),  $[2(2 + 2 -)1 + 1 -]$  ( $C_{11}$ ),  $[3 + 3 - 1 + 1 -]$  ( $D_{11}$ ), and  $[4 + 4 - 1 + 1 -]$  ( $E_{11}$ ). The names in parentheses give short abbreviations of the consecutive systems and the subscript indicates the total number of segments.

The chains  $A_{11}$  are characterized by uniform distribution of the charges, while for the system  $B_{11}$  the oppositely charged segments are grouped into two blocks (thus, the part of the chain non-bonded to the surface is a diblock polyampholyte). The remaining systems correspond to different “intermediate stages” between the systems  $A_{11}$  and  $B_{11}$ .

Figure 1(a) illustrates the influence of a small amount of tethered chains,  $R_C$ , on adsorption isotherms,  $a_\eta^* = a_\eta \sigma^2$ , of ions on a surface modified with  $A_{11}$  chains,

$$a_\eta = \int_0^\infty dz [\rho^{(\eta)}(z) - \rho_b^{(\eta)}]. \quad (28)$$

The adsorption isotherms are plotted versus the reduced bulk density of ions,  $\rho_b^{(\eta)*} = \rho_b^{(\eta)} \sigma^3$ . For  $R_C \rightarrow 0$ , the isotherms of cations and anions become identical, but the presence of even a small amount of tethered chains,  $R_C = 0.0005$ , leads to selective adsorption: anions are “more repelled” from the surface layer. For higher values of  $R_C$  the difference between anion and cation adsorptions increases, but the excess adsorptions become negative, especially at higher bulk ionic densities. This is due to the fact that when  $R_C$  increases, the volume within the surface layer available to ionic species decreases. However, at very low bulk densities a positive adsorption of cations is observed.

The effect of the architecture of chains on selectivity of adsorption of ionic species is illustrated in Fig. 1(b). The surface density of chains is kept constant and equal to 0.0025. The strongest positive excess adsorption of cations is for the chains  $B_{11}$ , i.e., when equally charged segments are grouped into blocks of 5 segments. The charge of the “outer” block is negative and this decides about stronger adsorption of cations. The architecture of the chains  $E_{11}$  is similar to the architecture of the chains  $B_{11}$ . Indeed, the plots of the adsorption isotherms for the former system are similar as for the system  $B_{11}$ . Among all the systems under study the architecture of the chains  $C_{11}$  is the closest to that of  $A_{11}$  and the isotherms of ions for both these systems are similar.

It is also of interest to compare the first moment of the total segment density profile,  $\langle z \rangle^* = \langle z \rangle / \sigma$ ,

$$\langle z \rangle = \int_0^{(M-1)\sigma + \sigma/2} dz z \rho_s^{(C)}(z) \quad (29)$$

for chains of different architecture. Note that the brush height is usually<sup>60</sup> defined as  $h = \alpha \langle z \rangle$ , where  $\alpha = 2$ , but according to some approaches<sup>61,62</sup>  $\alpha = 8/3$ .

At higher bulk densities of ions the differences between the values of  $\langle z \rangle^*$  for different architectures of chains are small. However, at lower  $\rho_b^{(\eta)*}$ , the values of  $\langle z \rangle^*$  can either increase or decrease with  $\rho_b^{(\eta)*}$ , depending on the architecture of chains. In the case of the system  $A_{11}$  the chains are the most

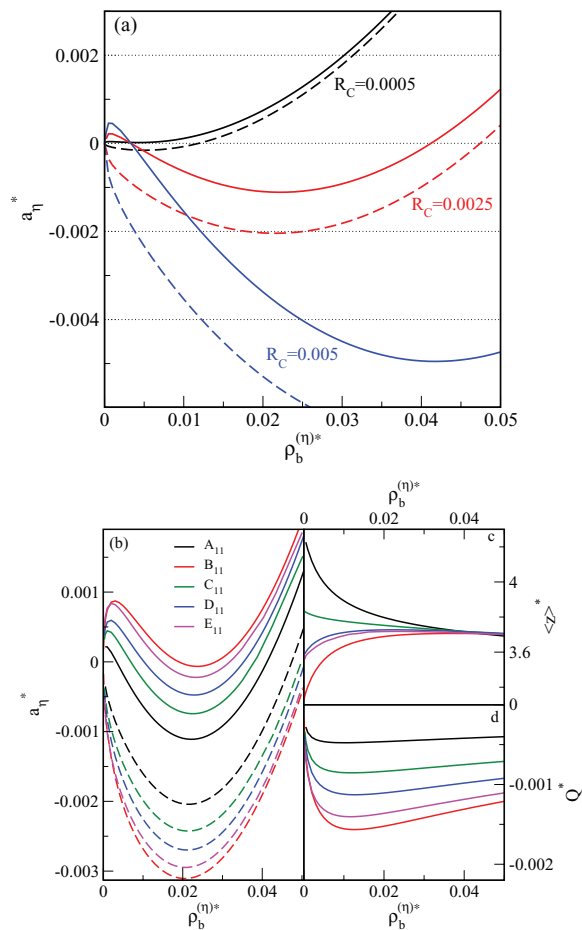


FIG. 1. Part (a): Excess adsorption isotherms of cations (solid lines) and anions (dashed lines) for different surface densities of the chains  $A_{11}$ . The numbers in the figure give the values of  $R_C$ . Parts (b)–(d) compare the effects of the architecture of tethered chains on adsorption isotherms (part (b)), on the first moment of the segment density profile (part (c)) and on the charge at the wall (part (d)). The surface density of tethered chains is  $R_C = 0.0025$ . Different colors correspond to different architectures, as indicated in part (b).

stretched at very low bulk densities, whereas for the architecture  $B_{11}$ —they are the most collapsed. For the chains  $C_{11}$ , the changes of  $\langle z \rangle^*$  with the concentration of ions are small (see Fig. 1(c)).

Part (d) of Fig. 1 shows the reduced charge at the wall,  $Q^* = Q \sigma^2$ ,

$$-Q = \sum_{i=1}^M \int_0^\infty dz Z_i^{(C)} \rho_i^{(C)}(z) + \sum_{\alpha=1}^2 \int_0^\infty dz Z_1^{(\alpha)} \rho^{(\alpha)}(z). \quad (30)$$

The strongest charge is for the  $B_{11}$  architecture, while the weakest—for the architecture  $A_{11}$ . In all cases the charge at the wall is negative. Of course, the charge is zero for  $\rho_b^{(\eta)*} = 0$ . If the bulk density increases, the wall charge quickly drops first and at a small  $\rho_b^{(\eta)*}$  attains a minimum. Next, it increases slowly, but even at a high bulk density it is still non-zero. It results from performed calculations that if all but the pinned segments are charged and if the resultant charge of the chain is zero, the sign of the wall charge is opposite to the sign of the charged segment that is directly attached to the pinned

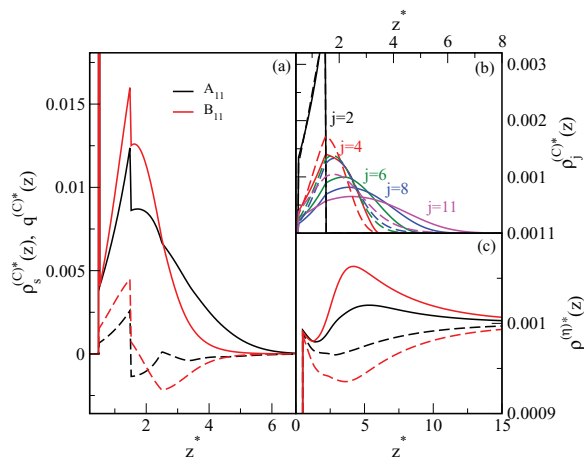


FIG. 2. Part (a) shows the total segment density profiles (solid lines) and the total charge, due to chains (dashed lines). Black and red colors correspond to the architectures  $A_{11}$  and  $B_{11}$ , respectively. Part (b) displays the individual segment density profiles,  $\rho_j^{(C)*}(z)$  for  $j = 2, 4, 6, 8,$  and  $11$ . Solid lines are the results for the architecture  $A_{11}$ , while dashed lines—for the architecture  $B_{11}$ . Part (c) shows the density profiles of cations (solid lines) and anions (dashed lines) for two considered architectures. All the calculations have been carried out for  $R_C = 0.0025$  and for  $\rho_b^{(n)*} = 0.001$ .

segment. We recall that our calculations have been carried out assuming that the electrostatic potential at the wall is zero.

Figure 2 displays the local densities of chains ( $\rho_s^{(C)*}(z) = \rho_s^{(C)}(z)\sigma^3$  and  $\rho_j^{(C)*}(z) = \rho_j^{(C)}(z)\sigma^3$ ; parts (a) and (b) and of ions ( $\rho^{(n)*}(z) = \rho^{(n)}(z)\sigma^3$ ; part (c) for two architectures:  $A_{11}$  and  $B_{11}$ . Here  $z^* = z/\sigma$ . The bulk density of ions is low. The value of  $\rho_b^{(n)*}$  has been selected as approximately equal to the bulk density corresponding to strongest negative surface charge  $Q^*$ , cf. Fig. 1(d). The surface density of tethered chains is low,  $R_C = 0.0025$ . The total segment density profile for the system  $A_{11}$  is more “diffuse” than for the system  $B_{11}$ , indicating stronger tendency of the chains to be stretched in the former system. This tendency is also seen in Fig. 1(b), where selected density profiles of individual segments have been plotted. While the density profiles of the second segment,  $\rho_2^{(C)*}(z)$ , are almost identical for the systems  $A_{11}$  and  $B_{11}$ , the profiles of higher segments of the chains  $B_{11}$  are shifted toward lower  $z^*$  values, in comparison to the profiles for the chains  $A_{11}$ .

In Fig. 2(a) we also show the charge profiles, resulting from the charges of segments,  $q^{(C)*}(z) = q^{(C)}(z)\sigma^3/e$ ,

$$q^{(C)}(z) = e \sum_{i=1}^M Z_i^{(C)} \rho_i^{(C)}(z). \quad (31)$$

For  $0.5 < z^* < 1.5$ , the charge  $q^{(C)*}(z)$  is positive. Despite of that, we do not observe any accumulation of anions within that region (Fig. 2(c)). The strongest accumulation of cations and, instantaneously, the strongest anions repelling take place within the region of  $1.5 < z^* < 7$ . In other words, the cations are adsorbed at and inside the “outer” part of the tethered chains.

We now consider how the length of tethered chains influences adsorption of ions. In Fig. 3(a), we show excess adsorption of cations (solid lines) and of anions (dashed lines)

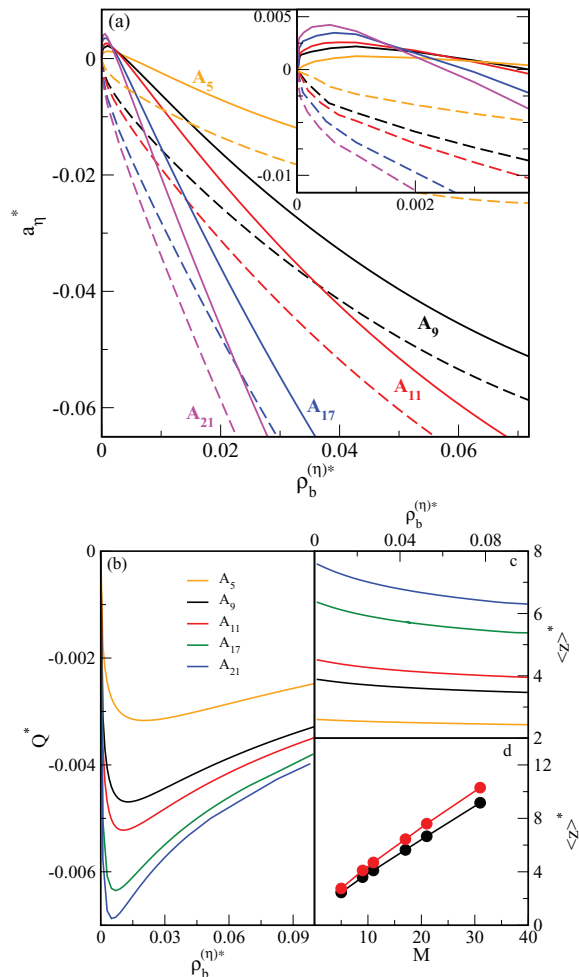


FIG. 3. Part (a): Adsorption isotherms of cations (solid lines) and anions (dashed lines) for the systems of architecture  $A_5, A_9, A_{11}, A_{17},$  and  $A_{21}$ . In each case the grafting surface density is  $R_C = 0.025$ . The inset shows the region of low bulk densities. Parts (b) and (c) illustrate the dependence of the surface charge density,  $Q^*$  (part (b)) and of  $\langle z \rangle^*$  (part (c)) on the bulk density of ions for the systems from part (a). Part (d) shows the dependence of  $\langle z \rangle^*$  on the length of the chains for  $\rho_b^{(n)*} = 0.05$  (black line and circles) and for  $\rho_b^{(n)*} = 0.006$  (red line and symbols).

on the walls modified with tethered chains of different length. As usual, the first (pinned) segment is uncharged, while all the remaining segments bear alternate charges. The architectures under study include:  $[2(1 + 1 -)]$  ( $A_5$ ),  $[4(1 + 1 -)]$  ( $A_9$ ),  $A_{11}$ ,  $[8(1 + 1 -)]$  ( $A_{17}$ ), and  $[10(1 + 1 -)]$  ( $A_{21}$ ). The grafting density,  $R_C = 0.025$ , is now higher than in previous cases, therefore the positive excess adsorption of cations is observed only within the range of low bulk densities (see the inset to Fig. 3(a)). The maximum of excess adsorption of cations is at a very low bulk density,  $\rho_b^{(n)*} < 0.001$ . Within that region of bulk densities the cation adsorption is higher for longer chains. However, at higher bulk densities, the effects of volume exclusion of ions from the surface layer prevail and the excess adsorption is negative. Part (b) of Fig. 3 illustrates how the surface charge on the wall changes with the bulk density (left panel). The shape of the curves displayed here follows the shape of the curves in Fig. 1(b). An increase of the chain length causes that the minimum of  $Q^*$  becomes deeper and shifts toward lower bulk density. The minimum of the surface

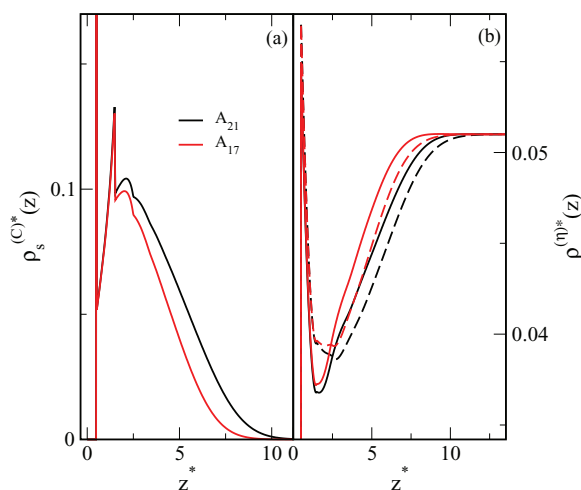


FIG. 4. A comparison of the total segment density profiles (part (a)) and of the profiles of cations (solid lines) and anions (dashed lines; part (b)) for the systems  $A_{17}$  (red lines) and  $A_{21}$  (black lines). The calculations are for  $R_C = 0.025$  and  $\rho_b^{(\eta)*} = 0.006$ .

charge is at bulk densities higher than the maximum of the cation adsorption observed in the inset to Fig. 3(a).

Figure 3(c) illustrates the changes of  $\langle z \rangle^*$  with the bulk density. For a set of chains with alternating charges of segments, an increase of  $\rho_b^{(\eta)*}$  causes a decrease of  $\langle z \rangle^*$  for all lengths of the chains,  $M$ . Part (d) shows the dependence of  $\langle z \rangle$  on the length of chains. Black curve in Fig. 3(d) has been evaluated for  $\rho_b^{(\eta)*} = 0.05$ , while the red one—for  $\rho_b^{(\eta)*} = 0.006$ , i.e., at the density close to that corresponding to the minima on the curves of  $Q^*$  versus  $\rho_b^{(\eta)*}$ . At a fixed bulk density the increase of  $\langle z \rangle^*$  with the chain length is almost linear. In fact, for  $\rho_b^{(\eta)*} = 0.05$  ( $\rho_b^{(\eta)*} = 0.006$ ) the slope of the linear correlation is 0.256 (0.288) and in both cases the squared correlation coefficient is as high as 0.9999. The values of the slope are much lower than 1 (the latter value is expected for fully stretched chains), therefore, for increasing  $M$  the chains become more twisted.

The structure of the interfacial layer for the systems  $A_{17}$  and  $A_{21}$  is shown in Fig. 4. Part (a) gives an insight into the structure of the chains, while part (b) displays the density profiles of cations (solid lines) and anions (dashed lines). The calculations have been carried out for a fixed surface grafting density and at the bulk density close to the minimum on the dependence of  $Q^*$  versus  $\rho_b^{(\eta)*}$ , cf. Fig. 3(b). We see that within the first and the second layers adjacent to the wall the structure of the chains is almost independent of their length. The main difference between the profiles for the chains built of 17 and 21 segments is that the tail of the profile for the latter system is shifted toward larger  $z^*$  values. At the investigated bulk density the excess adsorption of both ionic species is negative (cf. Fig. 3(a)). The accumulation of ions takes place only within the first adlayer (Fig. 4(b)) and the height of the first local density peaks of cations and anions is quite similar (this layer is also occupied by the uncharged segments of the chains). The difference between the negative excess adsorption isotherms of ionic species is due to stronger removal of anions from the layer occupied by segments of polymer.

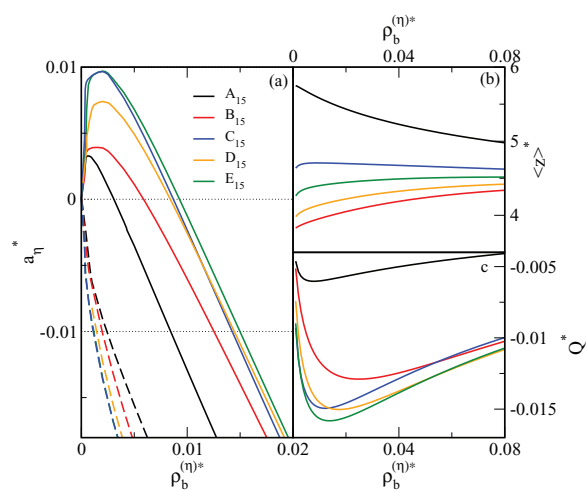


FIG. 5. Adsorption isotherms (part (a)), the dependence of  $\langle z \rangle^*$  versus the bulk density (part (b)) and the dependence of the surface charge  $Q^*$  on bulk density for the systems involving chains  $A_{15}$ – $E_{15}$  (for explanation see the text). The grafting density is  $R_C = 0.025$ .

The calculations presented above have demonstrated that the architecture of the chains decides about selectivity of adsorption of ionic species. So far the highest selectivity was observed for charged segments grouped into two blocks. However, it is still unclear whether this architecture really ensures the highest selectivity. Therefore, the next series of our calculations has been carried out for the systems with the chains built of more than two blocks of differently charged segments. We have studied the chains of  $M = 15$  segments with the following architectures:  $[7(1 + 1 -)]$  ( $A_{15}$ ),  $[7 + 7 -]$  ( $B_{15}$ ),  $[(4 + 4 -)3(1 + 1 -)]$  ( $C_{15}$ ),  $[6 + 6 - 1 + 1 -]$  ( $D_{15}$ ), and  $[5 + 5 - 2(1 + 1 -)]$  ( $E_{15}$ ).

Similarly as in previous cases, the selectivity of the ion adsorption is the lowest for the architecture  $A_{15}$ , i.e., when the consecutive segments are alternately charged (see Fig. 5(a)). However, the highest selectivity is for the systems  $C_{15}$  and  $E_{15}$ , not for the system  $B_{15}$ . The changes in adsorption selectivity are correlated with the charge at the wall,  $Q^*$  (cf. Fig. 5(c)). The highest negative surface charge is for the systems with the highest selectivity. However, there are no correlations between  $\langle z \rangle$  and the selectivity. For the brushes  $C_{15}$  and  $E_{15}$  the change of  $\langle z \rangle$  with bulk fluid density is small. Indeed, except for low bulk densities, the values of  $\langle z \rangle$  are almost constant for those systems. In the case of the brush  $A_{15}$  the values of  $\langle z \rangle$  decrease with the bulk density, while they increase for the brush  $B_{15}$  (Fig. 5(b)).

In Fig. 6 we show examples of the density profiles and of the total charge profile,  $q^*(z) = q(z)\sigma^3/e$ . The results are for rather high bulk densities of ionic species,  $\rho_b^{(\eta)*} = 0.05$ , and the excess adsorption of both ions is negative. There is a significant difference between the profiles for the system  $A_{15}$  and for all remaining systems. For the system  $A_{15}$  the profiles  $\rho^{(\eta)*}(z)$  are depleted for  $z^* > 1.5$ , while in the case of remaining systems an accumulation of the cations within the “outer” part of the brush takes place (Fig. 6(a)). The structure of electric “double layer” of the brush  $A_{15}$  also differs from all remaining brushes (Fig. 6(b)). Although in all cases the first layer,  $0.5 < z^* < 1.5$ , is positively charged (inspection



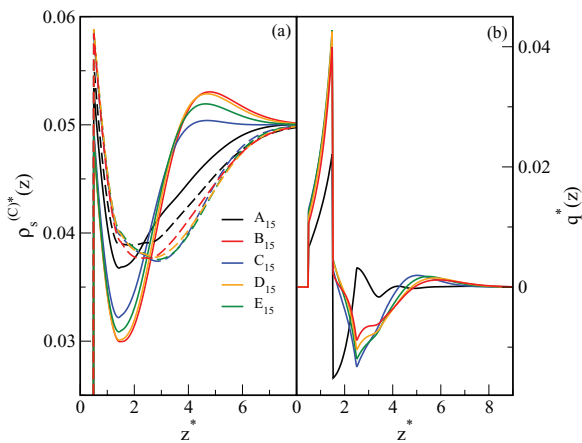


FIG. 6. Part (a): Density profiles of cations (solid lines) and of anions (dashed lines). Part (b): The total charge profiles,  $q^*(z)$ . The calculations are for the systems  $A_{15}$ – $E_{15}$  at the grafting density  $R_C = 0.025$  and for the bulk density of ions,  $\rho_b^{(\eta)*} = 0.05$ .

of the profiles of individual segments has indicated that this is mainly due to the positive charge of the  $j = 2$  segments), the structure of higher layers for the system  $A_{15}$  and the remaining systems is different. The secondary maximum of the positive charge for the system  $A_{15}$  is at  $z^* \approx 2.6$ , whereas at the same distance a maximum of the negative charge occurs for all remaining systems.

The location of the point of zero charge depends on the architecture of the chains, see Fig. 7. The PZC ( $V_{PZC}$ ) is the value of the electrostatic potential at the wall,  $V_0$ , at which the surface charge density is zero. Hereafter, the reduced potential at the wall is defined as  $V^* = eV_0/kT$ . For  $V^* = 0$  and for the length of chains studied by us the values of the surface density at the wall are small. As we have already mentioned, our calculations indicated that the sign of the surface charge at  $V^* = 0$  is opposite to the sign of the segment  $j = 2$  attached to the pinned segment. Therefore, the values of  $V_{PZC}^*$  are positive.

In Figures 7(a) and 7(b) we show how the charge at the wall depends on the architecture of the chains, on the surface grafting density and on the bulk density. Unfortunately, except for the statement: “all the calculations performed by us indicate that the values of PZC for the architecture with alternating charges of consecutive segments (i.e., for the architectures  $A_{11}$ ,  $A_{15}$ , etc.) are lower than for remaining architectures,” we are unable to provide an unequivocal statement which architecture leads to the highest value of  $V_{PZC}^*$ . Also, the influence of the bulk fluid density on  $V_{PZC}^*$  is not unequivocal. Except for the region of very low bulk fluid densities (of course,  $V_{PZC}^* \rightarrow 0$  for  $\rho_b^{(\eta)*} \rightarrow 0$ ), an increase of  $\rho_b^{(\eta)*}$  causes that  $V_{PZC}^*$  decreases, see Fig. 7(c). However, an increase of the surface grafting density  $R_C$  causes that  $V_{PZC}^*$  increases. At higher grafting densities this increase is almost linear, cf. Fig. 7(b). Note that the dependences of  $Q^*$  versus  $V^*$  (cf. Figs. 7(a) and 7(b)) are almost perfectly linear, thus for the investigated range of data the differential capacitance of the double layer,

$$C = dQ/dV \quad (32)$$

is independent of the electrostatic potential.

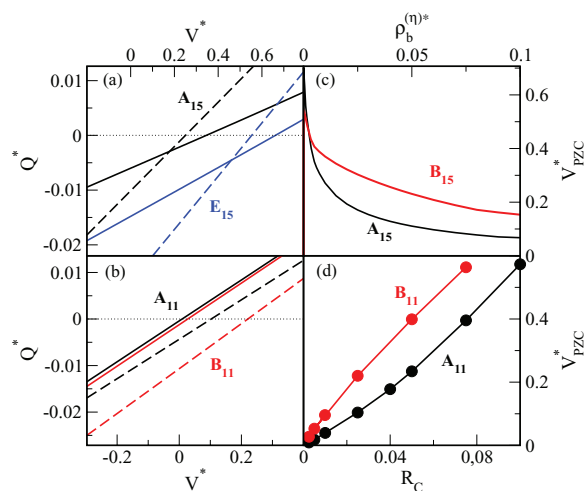


FIG. 7. Part (a):  $Q^*$  versus the electrostatic potential  $V^*$  for the systems  $A_{15}$  and  $E_{15}$  at  $R_C = 0.025$  and the bulk density  $\rho_b^{(\eta)*} = 0.006$  that is close to the bulk density at the minimum of the curves in Fig. 5(c) (solid lines) and at  $R_C = 0.05$  and  $\rho_b^{(\eta)*} = 0.05$  (dashed lines). Part (b) shows the curves  $Q^*$  versus  $V^*$  for the systems  $A_{11}$  and  $B_{11}$  (black and red lines, respectively),  $\rho_b^{(\eta)*} = 0.05$  and  $R_C = 0.0025$  (solid lines), and  $R_C = 0.025$  (dashed lines). Part (c) illustrates the dependence of  $V_{PZC}^*$  on the bulk density for the systems  $A_{14}$  and  $B_{15}$  at  $R_C = 0.025$ , while part (d) shows how  $V_{PZC}^*$  depends on  $R_C$  for the systems  $A_{11}$  and  $B_{11}$  (black and red lines, respectively).

Figure 8 shows examples of the dependence of the reduced differential double layer capacitance,  $C^* = dQ^*/dV^*$ , on the bulk fluid density (parts (a) and (b)) for systems involving chains of  $M = 11$  (part (a)) and of  $M = 15$  segments. Our calculations have indicated that for fixed length of the chains, the bulk fluid density and the surface density of tethered chains, the highest capacitance is for the systems in which the chains are built of two blocks of differently charged

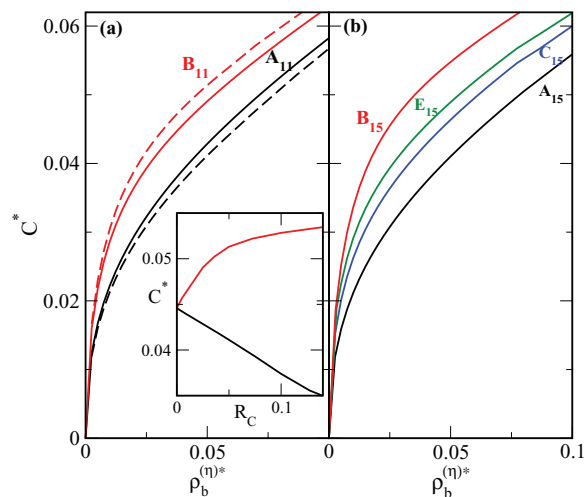


FIG. 8. The dependence of the double layer capacitance on the bulk density. Part (a) is for the tethered chains of  $M = 11$  segments at two values of  $R_C$ ,  $R_C = 0.025$  (solid lines), and  $R_C = 0.05$  (dashed lines). Part (b) is for  $M = 15$  and for  $R_C = 0.05$ . The architectures of the chains are given in the figure. The inset to part (a) shows the dependence of  $C^*$  on the grafting density for the systems  $A_{11}$  (black line) and  $B_{11}$  (red line). The bulk fluid density was  $\rho_b^{(\eta)*} = 0.05$ .

segments (i.e., for the chains of *B*-type). However, the capacitance is the lowest for the systems with alternately charged segments (*A*-type chains). With an increase of the surface grafting density,  $R_C$ , the double layer capacitance increases for the systems of *B*-type and decreases for the systems with alternately charged consecutive segments. Except for the two above cases, our calculations have not allowed for deriving any rule concerning the changes of the capacitance with  $R_C$  in the case of an arbitrary architecture. Also, we have not found any correlations between the changes of the double layer capacitance with the selectivity of adsorption of ions.

#### IV. SUMMARY

We proposed a version of the density functional theory to study adsorption of ions on surfaces modified by tethered polyampholytes. We considered the special case of strongly dissociated polyampholytes whose net resultant charge is zero, i.e., the numbers of positively and negatively charged segments were the same. The ionic solution was modeled in the framework of the so-called “weighted correlation approach- $k^2$ ” of Wang *et al.*<sup>56</sup>

Our principal aim was to check how the architecture of the chains influences the structure, adsorption (and selectivity of adsorption of particular ions), and electric properties of the double layer. We have concentrated on the region of rather low surface densities of tethered chains, because for higher grafting densities the excess adsorptions of both ionic species are negative. In all investigated cases the lowest selectivity exhibited the systems with the chains built of alternately charged segments. However, we were not able to find which architecture (for a given length of the chains) assures the highest selectivity of ions adsorption.

Differences in the architecture of chains lead to different changes of the brush height with the bulk fluid density. In general, for the chains built of alternately charged segments, the height of the brush decreases with the bulk fluid density, while in the case of chains built of blocks of segments of the same charge, an inverse effect of the bulk density is observed.

We have discussed the following properties of the electric double layer: the potential of zero charge and the double layer capacitance. Except for the region of very low bulk fluid densities, the potential of zero charge was the lowest for the chains with alternately charged segments. An increase of the chains length caused an increase of the potential of the zero charge. The double layer capacitance was the lowest for the systems with alternately charged chains and the highest when equally charged segments have been grouped into two blocks. In both these cases the dependence of the double layer capacitance on the grafting density was different: the capacitance decreased with an increase of  $R_C$  in the first case and increased in the second case.

#### ACKNOWLEDGMENTS

M.B. and S.S. acknowledge support from the Ministry of Science of Poland under the Grant No. N N204 151237. J.M.I. acknowledges support from EC under Grant No. PIRSES 268498.

- <sup>1</sup>A. V. Dobrynin, *Curr. Opin. Colloid Interface Sci.* **13**, 376 (2008).
- <sup>2</sup>T. Terabayashi, T. Maruyama, Y. Shimizu, M. Komatsu, and T. Takahashi, *J. Appl. Polym. Sci.* **101**, 4454 (2006).
- <sup>3</sup>A. Ciferri and S. Kudaibergenov, *Macromol. Rapid Commun.* **28**, 1953 (2007).
- <sup>4</sup>D. A. Hoagland, *Encyclopedia of Polymer Science and Engineering* (Wiley, New York, 2004).
- <sup>5</sup>S. Sanjuan and Y. Tran, *J. Polym. Sci. A* **46**, 4305 (2008).
- <sup>6</sup>F. Polzer, J. Heigl, C. Schneider, M. Ballauff, and O. V. Borisov, *Macromolecules* **44**, 1654 (2011).
- <sup>7</sup>A. B. Lowe and C. L. McCormick, *Chem. Rev. (Washington, D.C.)* **102**, 4177 (2002).
- <sup>8</sup>J. Jiang, J. Feng, H. Liu, and Y. Hu, *J. Chem. Phys.* **124**, 144908 (2006).
- <sup>9</sup>J. Feng, H. L. Liu, and Y. Hu, *Mol. Simul.* **32**, 51 (2006).
- <sup>10</sup>M. Baratlo and H. Fazli, *Eur. Phys. J. E* **29**, 131 (2009).
- <sup>11</sup>M. Baratlo and H. Fazli, *Phys. Rev. E* **81**, 011801 (2010).
- <sup>12</sup>L.-J. Qu, X. Man, C. C. Hant, D. Qiu, and D. Yan, *J. Phys. Chem. B* **116**, 743 (2012).
- <sup>13</sup>M. Das, N. Sanson, and E. Kumacheva, *Chem. Rev.* **20**, 7157 (2008).
- <sup>14</sup>Z. Zhang, J. A. Finlay, L. Wang, Y. Gao, J. A. Callow, M. E. Callow, and S. Jinag, *Langmuir* **25**, 13516 (2009).
- <sup>15</sup>S. M. Arifuzzaman, “Applications of functional polymer brushes for nanoparticle uptake and prevention of protein adsorption,” Ph.D. dissertation (North Carolina State University, Raleigh, North Carolina, 2010), see <http://www.lib.ncsu.edu/resolver/1840.16/6154>.
- <sup>16</sup>U. Raviv, S. Giasson, N. Kampf, J. F. Gohy, R. Jerome, and J. Klein, *Nature (London)* **425**, 163 (2003).
- <sup>17</sup>A. Kusumo, L. Bombalski, Q. Lin, K. Matyjaszewski, J. W. Schneider, and R. D. Tilton, *Langmuir* **23**, 4448 (2007).
- <sup>18</sup>F. Zhou, W. Shu, M. E. Welland, and W. T. S. Huck, *J. Am. Chem. Soc.* **128**, 5326 (2006).
- <sup>19</sup>*Polymer Brushes*, edited by R. C. Advincula, W. J. Brittain, K. C. Caster, and J. Rühle (Wiley-VCH, Weinheim, 2005).
- <sup>20</sup>A. Yethiraj, *J. Phys. Chem. B* **113**, 1539 (2009).
- <sup>21</sup>Z. D. Li and J. Z. Wu, *J. Phys. Chem. B* **110**, 7473 (2006); *Phys. Rev. Lett.* **96**, 048302 (2006).
- <sup>22</sup>L. Wang, H. Liang, and J.-Z. Wu, *J. Chem. Phys.* **133**, 044906 (2010).
- <sup>23</sup>J. F. Joanny, *J. Phys. II* **4**, 1281 (1994).
- <sup>24</sup>A. V. Dobrynin, M. Rubinstein, and J. F. Joanny, *Macromolecules* **30**, 4332 (1997).
- <sup>25</sup>N. P. Shusharina and P. Linse, *Eur. Phys. J. E* **4**, 399 (2001); **6**, 147 (2001).
- <sup>26</sup>A. Akinchina, N. P. Shusharina, and P. Linse, *Langmuir* **20**, 10351 (2004).
- <sup>27</sup>R. Messina, *Eur. Phys. J. E* **22**, 325 (2007).
- <sup>28</sup>J. McNamara, C. Y. Kong, and M. Muthukumar, *J. Chem. Phys.* **117**, 5354 (2002).
- <sup>29</sup>C. E. Woodward, *J. Chem. Phys.* **94**, 3183 (1991).
- <sup>30</sup>M. A. Carignano and I. Szleifer, *J. Chem. Phys.* **102**, 8662 (1995).
- <sup>31</sup>J. D. McCoy, M. A. Teixeira, and J. G. J. Curro, *J. Chem. Phys.* **117**, 2075 (2002).
- <sup>32</sup>Y. Ye, J. D. McCoy, and I. G. J. Curro, *J. Chem. Phys.* **119**, 555 (2003).
- <sup>33</sup>Y.-X. Yu and J.-Z. Wu, *J. Chem. Phys.* **117**, 2368 (2002); **117**, 10156 (2002); **118**, 3835 (2003).
- <sup>34</sup>D. P. Cao and J.-Z. Wu, *Langmuir* **21**, 9786 (2005); **22**, 2712 (2006).
- <sup>35</sup>D. P. Cao and J.-Z. Wu, *J. Chem. Phys.* **121**, 4210 (2004).
- <sup>36</sup>Z. D. Li, D. P. Cao, and J.-Z. Wu, *J. Chem. Phys.* **122**, 174708 (2005).
- <sup>37</sup>T. Jiang, Z. D. Li, and J.-Z. Wu, *Macromolecules* **40**, 334 (2007).
- <sup>38</sup>X. Xu and D. P. Cao, *Soft Matter* **6**, 4631 (2010).
- <sup>39</sup>M. Borówko, W. Rzyśko, S. Sokołowski, and T. Staszewski, *J. Chem. Phys.* **126**, 214703 (2007).
- <sup>40</sup>M. Borówko, A. Patrykiewicz, S. Sokołowski, and T. Staszewski, *Collect. Czech. Chem. Commun.* **75**, 221 (2010).
- <sup>41</sup>M. S. Wertheim, *J. Stat. Phys.* **35**, 19–35 (1984); **42**, 477–492 (1986).
- <sup>42</sup>P. Bryk and L. G. MacDowell, *J. Chem. Phys.* **135**, 204901 (2011).
- <sup>43</sup>P. Bryk, O. Pizio, and S. Sokołowski, *J. Chem. Phys.* **122**, 174906 (2005).
- <sup>44</sup>T. G. Smagala, A. Patrykiewicz, S. Sokołowski, O. Pizio, and W. R. Fawcett, *J. Chem. Phys.* **128**, 024907 (2008).
- <sup>45</sup>Z. Tang, L. E. Scriven, and H. T. Davis, *J. Chem. Phys.* **97**, 9258 (1992).
- <sup>46</sup>R. Kjellander and H. Greberg, *J. Electroanal. Chem.* **450**, 233 (1998).
- <sup>47</sup>C. N. Patra and A. Yethiraj, *J. Phys. Chem. B* **103**, 6080 (1999).
- <sup>48</sup>D. Boda, D. Henderson, R. Rowley, and S. Sokołowski, *J. Chem. Phys.* **111**, 9382 (1999).

- <sup>49</sup>Y.-X. Yu, J.-Z. Wu, and G.-H. Gao, *J. Chem. Phys.* **120**, 7223 (2004).
- <sup>50</sup>D. Gillespie, W. Nonner, and R. Eisenberg, *Phys. Rev. E* **68**, 031503 (2003).
- <sup>51</sup>O. Pizio, A. Patrykiewicz, and S. Sokołowski, *J. Chem. Phys.* **121**, 11957 (2004).
- <sup>52</sup>E. Waisman and J. L. Lebowitz, *J. Chem. Phys.* **56**, 3093 (1972).
- <sup>53</sup>D. Gillespie, *J. Chem. Phys.* **134**, 044103 (2011).
- <sup>54</sup>O. Pizio and S. Sokołowski, *J. Chem. Phys.* **122**, 144707 (2005).
- <sup>55</sup>J. Reszko-Zygmunt, S. Sokołowski, D. Henderson, and D. Boda, *J. Chem. Phys.* **122**, 084504 (2005).
- <sup>56</sup>Z. Wang, L. Liu, and I. Neretnieks, *J. Phys.: Condens. Matter* **23**, 175002 (2011); *J. Chem. Phys.* **135**, 244107 (2011).
- <sup>57</sup>J. Jiang, L. Blum, O. Bernard, and J. M. Prausnitz, *Mol. Phys.* **99**, 1121 (2001).
- <sup>58</sup>J. Jiang, L. Blum, O. Bernard, J. M. Prausnitz, and S. L. Sandler, *J. Chem. Phys.* **116**, 7977 (2002).
- <sup>59</sup>Yu. V. Kalyuzhnyi, M. F. Holovko, and V. Vlachy, *J. Stat. Phys.* **100**, 243 (2000).
- <sup>60</sup>C. Pastorino, K. Binder, and M. Müller, *Macromolecules* **42**, 401 (2009).
- <sup>61</sup>T. Kreer, S. Metzger, M. Müller, K. Binder, and J. Baschnagel, *J. Chem. Phys.* **120**, 4012 (2004).
- <sup>62</sup>A. Milchev and K. Binder, *Macromol. Symp.* **252**, 47 (2007).